Downloaded from orbit.dtu.dk on: Jun 22, 2025

DTU Library

Optimal tuning of model predictive controllers for organic Rankine cycle systems recovering waste heat from heavy-duty vehicles

Pili, Roberto; Wieland, Christoph; Spliethoff, Hartmut; Haglind, Fredrik

Published in:
Applied Thermal Engineering

Link to article, DOI:
10.1016/j.applthermaleng.2022.119803

Publication date:
2023

Document Version
Publisher's PDF, also known as Version of record

Link back to DTU Orbit

Citation (APA):
Pili, R., Wieland, C., Spliethoff, H., & Haglind, F. (2023). Optimal tuning of model predictive controllers for organic Rankine cycle systems recovering waste heat from heavy-duty vehicles. *Applied Thermal Engineering*, *220*, Article 119803. https://doi.org/10.1016/j.applthermaleng.2022.119803

General rights
Copyright and moral rights for the publications made accessible in the public portal are retained by the authors and/or other copyright owners and it is a condition of accessing publications that users recognise and abide by the legal requirements associated with these rights.

- Users may download and print one copy of any publication from the public portal for the purpose of private study or research.
- You may not further distribute the material or use it for any profit-making activity or commercial gain
- You may freely distribute the URL identifying the publication in the public portal

If you believe that this document breaches copyright please contact us providing details, and we will remove access to the work immediately and investigate your claim.

Applied Thermal Engineering 220 (2023) 119803

Contents lists available at ScienceDirect

Applied Thermal Engineering

journal homepage: www.elsevier.com/locate/apthermeng

Research Paper

Optimal tuning of model predictive controllers for organic Rankine cycle systems recovering waste heat from heavy-duty vehicles

Roberto Pili [a,*], Christoph Wieland [b], Hartmut Spliethoff [b,c], Fredrik Haglind [a]

[a] Technical University of Denmark, Department of Mechanical Engineering, Kgs. Lyngby, Denmark
[b] Technical University of Munich, Chair of Energy Systems, Garching bei München, Germany
[c] Bavarian Center for Applied Energy Research, Garching bei München, Germany

A B S T R A C T

The organic Rankine cycle power system is an emerging technology, which is able to recover the waste heat from the diesel engine of heavy-duty trucks and thus increase the overall engine efficiency. One of the major technical challenges for the integration of the organic Rankine cycle unit on-board trucks are the broad and rapid fluctuations of the available waste heat, caused by the unsteady driving conditions of the truck. Model predictive control has shown to be a powerful tool to ensure safe operation and optimal performance of the organic Rankine cycle unit on-board trucks. This paper presents a novel systematic method for the tuning of model predictive controllers based on a multi-objective optimization routine using a fourth-order reduced linear model. The objectives of the optimization are the settling time due to a step change of the exhaust gas mass flow rate and the cumulative controller effort due to measurement noise. The results suggest that a trade-off exists between the two objectives. Among the controller design parameters, the input rate weight has the largest influence on the controller performance. Interestingly, the simplified optimization procedure based on the reduced-order linear model of the organic Rankine cycle unit can provide key information about the controller performance based on a more complex nonlinear model of the organic Rankine cycle unit when subjected to a realistic waste heat profile. The results indicate that the settling time due to a step change of the exhaust gas mass flow rate is a good indicator of the absolute mean square tracking error over the profile, and it should not exceed 15 s for an absolute mean square tracking error below 2 K. On the other hand, the cumulative controller effort due to measurement noise is strongly correlated to the cumulative controller effort over the profile, and it should stay below 0.5 %/s for a cumulative controller effort over the whole profile below 2 %/s. The presented method is a powerful tool to help the control designer to find the optimal design parameters of model predictive controllers in a systematic way, in contrast to the time-consuming, experience-based trial and error methods.

1. Introduction

More than 50 % of the fuel energy consumed by the diesel engines of heavy-duty trucks is released unused to the environment in the form of low to medium temperature waste heat, thus contributing to high fuel consumption and carbon dioxide emissions [1]. Especially in the last two decades, researchers have focused on the organic Rankine cycle (ORC) technology as a solution to recover the waste heat available from the truck diesel engines. Teng et al. [2] pointed out that the exhaust gases are the main source of interest for waste heat recovery, while the engine coolant is less favorable because of its low temperature. Park et al. [3] analyzed the waste heat recovery from a 10.8L diesel engine and demonstrated a 3–5 % fuel saving by using an ORC with ethanol as working fluid. Wang et al. [4] investigated the performance of nine organic working fluids recovering heat from a vehicle engine. The results showed that R245fa and R245ca were the most environmental-friendly working fluids among the investigated ones with thermal efficiencies between 8 and 10 %. Dolz et al. [5] studied the integration of a bottoming Rankine cycle in a 12L heavy-duty vehicle engine and reported fuel savings up to 16 %. Hountalas et al. [6] developed a simulation model for an ORC unit recovering heat from the exhaust gas tailpipe, the exhaust gas recirculation cooler and the charge air cooler. The results suggested that fuel savings between 9 % and 11 % are feasible.

One of the main challenges for the waste heat recovery are the large and rapid fluctuations of the mass flow rate and temperature of the waste heat caused by the unsteady driving conditions of the truck. In order to cope with these, increasing efforts have been dedicated to the design of the ORC unit considering the dynamic behavior of the ORC system and to the development of control strategies for the ORC unit [7–9]. Jimenez-Arreola et al. [10] studied the dynamic behavior of two types of ORC evaporators subjected to fluctuating waste heat. The waste heat fluctuations can be dampened considerably by using larger tube diameters and smaller cross-sectional areas on the exhaust gas side for fin-and-tube heat exchangers, while larger port diameters provide larger thermal inertia in lover fin multi-port flat tube heat exchangers. The work in Ref. [10] was further extended by Carraro et al. [11] who

* Corresponding author.
E-mail address: robpi@mek.dtu.dk (R. Pili).

https://doi.org/10.1016/j.applthermaleng.2022.119803
Received 4 April 2022; Received in revised form 21 August 2022; Accepted 30 November 2022
Available online 5 December 2022
1359-4311/© 2022 The Authors. Published by Elsevier Ltd. This is an open access article under the CC BY license (http://creativecommons.org/licenses/by/4.0/).

Nomenclature

Symbols

A	Surface area [m^2]
A	State matrix [-]
B	Input state matrix [-]
C	Output state matrix [-]
c_p	Specific heat at constant pressure [J/kgK]
c_W	Specific heat of solid material (wall) [J/kgK]
D	Output feed-through matrix [-]
d	Disturbance [-]
d	Tube outer diameter [m]
d_f	Fin outer diameter [m]
Δ	Variation [-]
E	Disturbance state matrix [-]
F	Disturbance output matrix [-]
f	State function [-]
f_{pitch}	Fin pitch [m]
g	Output function [-]
h	Specific enthalpy [J/kg]
J	Cost function [-]
k	Controller proportional constant [1/Pa]
k_T	Turbine constant [$kg/sK^{0.5}/Pa$]
l	Tube length [m]
M	Mass [kg]
$\dot{m}$	Mass flow rate [kg/s]
N_c	Control horizon [-]
N_p	Prediction horizon [-]
n_{tubes}	Number of heat exchanger tubes [-]
P	Power [W]
p	Pressure [Pa]
$\dot{Q}$	Heat transfer rate [W]
Q	Cumulative controller effort [1/s]
R	Thermal resistance [K/W]
SH	Degree of superheating [K]
s	Fin thickness [m]
T	Temperature [K]
t	Time [s]
V	Volume [m^3]
x	State [-]
y	Output [-]
Z	Compressibility factor [-]

Greek symbols

α	Heat transfer coefficient [W/m^2K]
γ	Ratio of specific heats [-]
η	Efficiency [-]
ρ	Density [kg/m^3]

Superscripts and subscripts

$\dot{}$	time derivative
*	steady state (operating point)
eg	exhaust gas
F	working fluid
f	fins/finned
in	inlet/input
o	outer bare (surface area)
out	outlet/output
SP	set point
w	Wall
wf	working fluid

Abbreviations

ARMSTE	Absolute Root Mean Square Tracking Error
EPSAC	Extended Prediction Self-Adaptive Control
MPC	Model Predictive Control
ORC	Organic Rankine Cycle
P	Pump
PI	Proportional Integral (control)
PID	Proportional Integral Derivative (control)
SISO	single-input–single-output (controller)
T	Turbine

analyzed the impact of the design of a fin-and-tube ORC evaporator over a 45-min waste heat profile of the exhaust gas of a heavy-duty vehicle engine. The authors reported that a suitable design of the tube inner parameter and tube spacing could reduce the fluctuations in ORC power output by 11 %. Tillmanns et al. [12] developed a working fluid selection routine that considers the dynamic behavior of the ORC unit. The best working fluids were short-chained hydrocarbons. It was also shown that a steady-state design routine based on the mean value of the waste heat conditions would overestimate the net power output of the ORC unit up to 30 %. Pili et al. [13] integrated the dynamic behavior of the ORC unit in the design optimization routine and compared the performance of different working fluids. It was found that the design degree of superheating at turbine inlet needs to be considerably higher when the dynamic behavior of the ORC unit is considered compared to a steady-state optimization. This is necessary to ensure a positive degree of superheating and avoid turbine damage. The same occurs if the outlet temperature of the exhaust gas is not allowed to drop excessively to avoid acidic condensation and corrosion of the exhaust system. Additional works on the waste heat recovery from heavy-duty vehicles can be found in Refs. [14] and [15].

In particular, the control of the ORC unit has the unique tasks of ensuring safe operation while maximizing the net power output. Recent reviews [8,9,16] highlighted the various control concepts suggested in literature, including conventional proportional-integral (PI) and proportional-integral-derivative (PID) controllers, feedback/feedforward schemes, linear quadratic control, non-Gaussian control, dynamic programming and model predictive control (MPC). Quoilin et al. [7] compared three PI control strategies for a small-scale ORC unit with a volumetric expander. The authors found that an expander speed controller regulating for an optimized temperature of the working fluid at expander inlet could achieve the highest overall efficiency of 6.6 %. Jolevski et al. [17] studied the interactions among the ORC actuators (pump speed, turbine throttle valve and coolant flow rate) and the controlled variables (pressure and temperature at turbine inlet and condenser outlet) by using non-square and dynamic square relative gain array techniques. Once the main interactions were found, single-input–single-output PI controllers were designed and tested. Marchionni et al. [18] investigated PI control strategies for a 40 kW ORC unit and highlighted that control strategies that manipulated the pump speed are able to maintain the net power output closer to the design point compared to options to manipulate the turbine speed. Lin et al. [19] considered PID control strategies to compare the usage of an oil storage system to dampen the waste heat fluctuations, finding out the acidic condensation of the exhaust gas might be more critical with the oil storage configuration. Yang et al. [20] used a PID control system coupled with a supervisory system that optimizes the cycle efficiency online and provides the optimal evaporation and condensation pressures. In this way, the control system could minimize downtime and keep the degree of superheating at turbine inlet always in the range between 5 K and 15 K. A technique to deal with disturbance rejection

given by the fluctuations in waste heat is to couple a feedforward action to the PI/PID feedback control loop. Padula et al. [21] proved the effectiveness of adding a static feedforward part to control the turbine speed by manipulating the turbine throttle valve and thus reject disturbances in electric load. A dynamic feedforward was developed by Peralez et al. [22] based on a reduced-order model of the ORC evaporator. The maximum deviation in degree of superheating at turbine inlet was reduced from 6.5 K to 1.9 K. Usman et al. [23] added a linear feedforward and a lead-lag compensator to a PI controller to reject disturbances in the turbo-generator speed by manipulating the speed of the ORC pump. The proposed control strategy was able to reduce the disturbance clearance time by 50 % compared with the only PI controller. Keller et al. [24] compared a static feedforward/PID controller with an MPC. The controllers act on the pump speed to control the temperature of the working fluid at expander inlet. The MPC outperformed the feedforward/PID scheme by limiting the deviations in setpoint within 5 K. Vaupel et al. [25] compared a linear feedforward model with a nonlinear model predictive control to highlight that the feedforward controller achieved marginally worse results than the more computationally-intensive nonlinear model predictive controller. Seitz et al. [26] developed a reduced-model feedforward and combine it with a PI and a linear quadratic controller. The feedforward combined with a gain-scheduled linear quadratic controller provided the best performance, although the deviations of the degree of superheating from the setpoint were relatively large (-15/+60 K). Further developments of nonlinear feedforward/feedback controllers were carried out by Pili et al. [27], where novel approximations were introduced to cope with the nonlinearity of high-order dynamic models of the ORC evaporator. Linear quadratic controllers were previously studied by Luong et al. [28] and compared with a PI controller. It was highlighted that the linear quadratic controller is particularly beneficial for multiple-input-multiple-output systems. Another class of advanced controllers are nonlinear Gaussian controllers (NGC), which solve an online multi-objective optimization problem to minimize the entropy function and the mean value of the squared tracking error, by assuming a non-Gaussian disturbance. Zhang et al. [29] developed a NGC for an ORC unit and compared it with a PID controller. Subjecting the ORC unit to a 5 K step change in the degree of superheating set point, the NGC showed better performance than the PID controller, reaching the set point faster with a lower overshoot. Zhang et al. [30] improved the formulation of the entropy of the tracking error by means of a quantized approach in order to reduce the computational burden. The particle swarm optimizer was used to find the optimal control input in each time step. The proposed solution could outperform a PID controller in terms of set point tracking, yet no information was reported about the computational time and real-time feasibility of the NGC solution. An online optimization problem was also solved by Peralez et al. [31], who implemented a dynamic programming algorithm to an ORC unit recovering waste heat from a train diesel engine. An adaptive grid algorithm was compared with a standard level-set algorithm, and it was found that the optimal control problem with adaptive grid was solved with reduced computational time and sufficient accuracy with respect to a more original level-set control problem. Because of the high computational effort strong or the significant model simplifications required, neither NGC nor dynamic programming has yet been extensively used in the control of ORC systems.

Several works suggest that MPC is a very powerful tool to ensure safe operation of the ORC unit and maximize its net power output, especially in comparison to traditional PID controllers. Among its advantages, MPC can easily handle multi-variable systems, reject measured and unmeasured disturbances, systematically account for plant mismatches and inherently deal with system constraints, which are crucial features to ensure operational and safety limits. Feru et al. [32] compared a conventional PI controller with linear and nonlinear MPC and concluded that the MPC concepts could lead to 15 % more recovered thermal energy over a cold-start World Harmonized Transient Cycle than the conventional PI control strategy. Grelet et al. [33] developed an explicit-model multi-model MPC formulation based on first-order-plus-time-delay models. The controller scheme could achieve good tracking performance when subjected to step changes in the set point. Hernandez et al. [34] developed a multiple-input multiple-output MPC using the Extended Prediction Self-Adaptive Control (EPSAC) algorithm [35]. The controller acted on the rotational speeds of the pump and expander to control the evaporation temperature and the degree of superheating. A comparison with a PI controller showed that the MPC achieved a higher net electrical output power and higher efficiency of the cycle. The EPSAC-MPC (this time only single-input–single-output) was then tested experimentally in Ref. [36], confirming the benefits of the MPC compared with the PI controller. The same research group later developed a perturbation-based extremum-seeking algorithm coupled to a low-level MPC and compared the performance with two PI control schemes [37]. The net electrical energy produced with the MPC was 12 % higher than the net electrical energy produced by the PI controllers. In a recent publication of Hernandez et al. [38] a multi-model MPC was tested experimentally in an 11-kW ORC unit allowing for an increase in net power output by 6 % when operating to the minimum allowed degree of superheating. A multi-model MPC was developed by Zhang et al. [39] by dividing the ORC operational range in three regions. The MPC showed good set point tracking and disturbance rejection performance. Pierobon et al. [40] developed a MPC for an offshore power station, where an ORC unit is combined to three gas turbines. The numerical results suggested that the MPC could limit the reduction of frequency up to 40 % for a load increase of 4 MW, compared to a PI control system. Luong et al. [41] tested a MPC for an ORC unit recovering transient waste heat from a heavy-duty diesel engine. The comparison with a PI and a linear quadratic integrator indicated that the MPC could reach the lowest deviations from the set point. Liu et al. [42] compared an MPC and a nonlinear MPC to a classical PID system for an ORC unit recovering waste heat from a heavy-duty diesel engine. The MPC demonstrated a more accurate temperature control and improved disturbance rejection. Koppauer et al. [43] developed a gain-scheduled MPC formulation coupled with an extended Kalman filter for state estimation. The solution showed good set point tracking capabilities and good robustness against model uncertainties.

Given the nonlinear nature that characterizes the dynamic behavior of ORC systems, other authors focused on nonlinear MPC options. In addition to the aforementioned Refs. [25,42,43], Rathod et al. [44] numerically and experimentally tested a nonlinear MPC coupled with an Extended Kalman Filter as a state estimator. The controller acted on the pump speed of an ORC unit recovering waste heat from a heavy-duty diesel engine. The results showed that the deviations of the degree of superheating from the set point were kept within 8 K for fast variations of the engine load point. The ACADO toolkit [45] was used in order to keep the computational time for the nonlinear MPC limited. Although gains in performance can be achieved, nonlinear MPCs require higher development costs and computational effort than the linear MPC. In addition, nonlinear MPC requires more powerful hardware and higher probability of controller failure because of the complexity of the underlying models.

The aforementioned works on MPC highlight the potential of the MPC concepts to control ORC power systems subjected to highly transient conditions, minimizing the deviations of the controlled variable from the desired set point and guaranteeing safe operation. However, in previous works the tuning of the MPC design parameters was in all cases based on trial and error procedures, potentially leading to suboptimal solutions and instability issues. In contrast to previous works on MPC for ORC systems, this paper focuses on the optimization of the MPC design parameters, thus allowing for the exploitation of the full potential of the MPC solution. A novel systematic method is presented for the tuning of model predictive controllers based on a multi-objective optimization routine written in MATLAB®/Simulink® [47] using a fourth-order reduced linear model. The MPC design is evaluated not only in terms

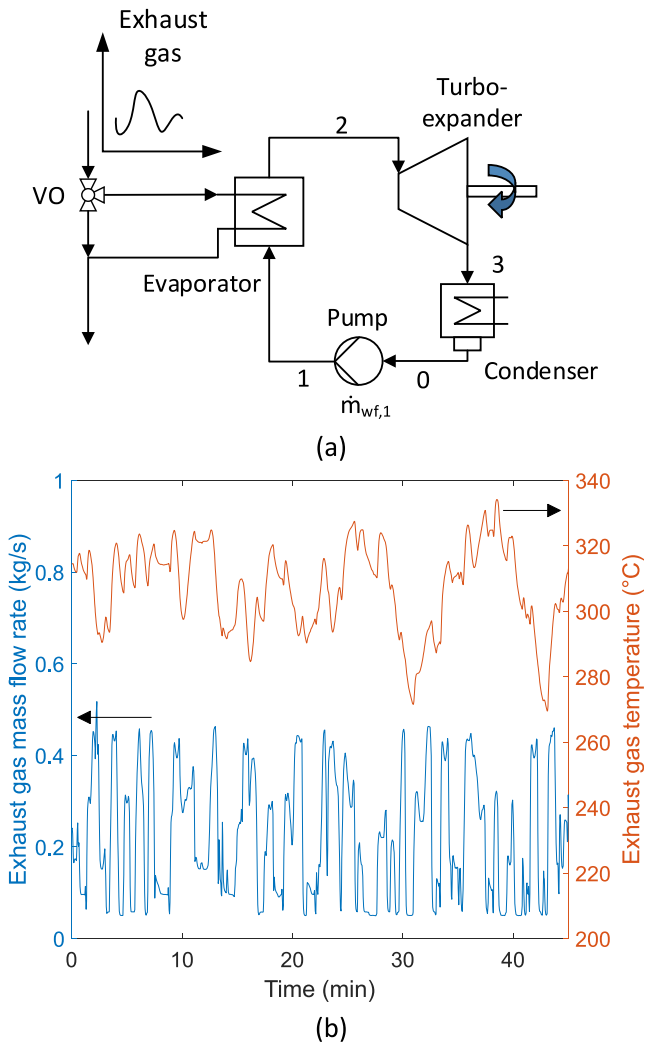

Fig. 1. (a) Layout of the ORC unit and (b) mass flow rate and temperature of the exhaust gas.

of disturbance rejection capabilities, but also in terms of cumulative controller effort and sensitivity to measurement noise, ensuring at the same time sufficient stability margins. The results of the optimization are numerically evaluated on a nonlinear model of an ORC unit subjected to a realistic waste heat profile from the tailpipe exhaust gas of a heavy-duty truck provided by a truck manufacturer.

The case study is presented in section 2, while section 3 presents the model development used for the MPC design. A sensitivity analysis is presented in section 4, together with a description of the multi-objective optimization routine. The optimization results follow in section 5 and the conclusions are presented in section 6.

2. Case study

The investigated system is a subcritical ORC unit without recuperator, whose heat source is the available waste heat in the exhaust gas of a 450-hp 13L turbocharged diesel engine of a heavy-duty truck. The plant layout is shown in Fig. 1a. The pump forwards the working fluid from liquid state at state 0 to the evaporator inlet at state 1. In this component, the working fluid is preheated, vaporized and superheated to state 2 by receiving heat from the engine exhaust gas. The vapor at state 2 expands in a turbo-expander generating mechanical power. An axial-flow turbine is selected here as the ORC-expander because of its potential for high isentropic efficiency [48,49], although other types of expander have been considered in other studies [50–53]. The turbine

Table 1
Decision variables for thermodynamic design optimization [11].

Quantity	Symbol	Unit	Lower bound	Upper bound
Mass flow rate	$\dot{m}_{wf,1}$	kg/s	0.01	10
Evaporation pressure	$p_{wf,2}$	bar	1.0	80 % $p_{wf,C}$*
Condensing temperature	$T_{wf,0}$	°C	20	60
Degree of superheating	$SH_{wf,2}$	K	3	40

* Critical pressure of R245fa: $p_{wf,C}$= 36.51 bar.

exhaust vapor at state 3 is then condensed back to liquid state (state 0) by rejecting heat to a cooling medium. Two actuators control the operation of the ORC system: i) the mass flow rate of the pump $\dot{m}_{wf,1}$ (or, in practice, its rotational speed) is manipulated to control the degree of superheating at turbine inlet $SH_{wf,2}$, and ii) a bypass valve opening VO on the exhaust gas stream (0: fully closed, 1: fully open) limits the turbine inlet pressure $p_{wf,2}$ to assure a pressure limit of 35 bar, thus preventing supercritical operation and excessive stress on the materials. The ORC unit uses R245fa as working fluid, due to its low flammability and high thermal degradation temperature of 300 °C [54].

The time profile of the engine exhaust gas is shown in Fig. 1b; the raw data may be found in Ref. [27]. The mass flow rate of the engine exhaust gas $\dot{m}_{eg}$ fluctuates very rapidly between 0.05 kg/s and 0.517 kg/s, whereas the inlet temperature $T_{eg,in}$ varies more slowly between 270 °C and 334 °C because of the dampening effect of the exhaust gas aftertreatment system (selective catalytic reactor).

The design of the ORC unit was carried out by using the code described in Ref. [11]. It is based on a steady-state thermodynamic optimization using the approximate time-weighted average of the exhaust gas mass flow rate and temperature (0.25 kg/s and 320 °C). The decision variables are reported in Table 1 with their lower and upper bounds. The objective function of the thermodynamic optimization (to be maximized) was the net power output, calculated as:

$$P_{net} = \dot{m}_{wf,1}\left[\left(h_{wf,2} - h_{wf,3}\right) - \left(h_{wf,1} - h_{wf,0}\right)\right] \quad (1)$$

where h_{wf} is the specific enthalpy of the working fluid. The states are indicated by the subscripts and follow the locations used in Fig. 1.

The design optimization assumed the isentropic efficiencies for the turbine and the pump to be 85 % and 75 %, respectively. The optimization led to the following nominal operating point for the ORC unit: a turbine inlet pressure $p_{wf,2}$ of 29.0 bar, a degree of superheating $SH_{wf,2}$ of 28.9 K, a condensation temperature of 56.7 °C (corresponding to a pressure $p_{wf,0}$ of 4.2 bar), and a mass flow rate $\dot{m}_{wf,1}$ of 0.187 kg/s. These variables led to a turbine mechanical power output of 6.8 kW and a nominal net mechanical power output of 6.1 kW.

Based on the thermodynamic design, the ORC evaporator was designed to estimate its heat transfer area (13.6 m^2), mass (42 kg) and volume (0.052 m^3), together with the nominal heat transfer coefficients of the working fluid and the exhaust gas. Given its high compactness, a cross-counterflow fin-and-tube heat exchanger was selected, where the working fluid flows inside the tubes and the exhaust gas flows on the finned tube outer side. The procedure for the design of the heat exchanger is described in detail in Ref. [11].

The results of the thermodynamic optimization (mass flow rates, temperatures and pressures) and heat exchanger design (heat transfer area, heat exchanger mass and volumes) were then used to develop a dynamic model of the high pressure part of the ORC unit, including the evaporator, the pump and the turbine with the software Dymola [55]. The dynamic models were developed by using the commercial library TIL [56] and then imported in MATLAB®/Simulink® [47] by using the functional mock-up interface [57]. The evaporator was discretized in the dynamic model by using 15 finite volume cells. The main equations describing the evaporator dynamics are the following:

$$\frac{d\left(V_{wf,i}\rho_{wf,i}\right)}{dt} = V_{wf}\left(\frac{\partial\rho_{wf,i}}{\partial h}\bigg|_p \frac{dh_{wf,i}}{dt} + \frac{\partial\rho_{wf,i}}{\partial p}\bigg|_h \frac{dp_{wf,i}}{dt}\right) = \dot{m}_{wf,in,i} - \dot{m}_{wf,out,i} \tag{2}$$

$$\frac{d\left(V_{wf,i}\rho_{wf,i}h_{wf,i} - V_{wf,i}p_{wf,i}\right)}{dt} = \dot{m}_{wf,in,i}h_{wf,in,i} - \dot{m}_{wf,out,i}h_{wf,out,i} + \dot{Q}_{wf,i} \tag{3}$$

where V_{wf} is the volume, ρ_{wf} is the density, p_{wf} is the pressure and $\dot{Q}_{wf}$ is the heat transfer rate of the working fluid. The subscripts 'in' and 'out' refer to the inlet and the outlet of the cell 'i'. An upwind discretization scheme was used, according to which the specific enthalpy of the cell is assumed equal to the specific enthalpy of the fluid leaving the cell. It is also accounted for fluid reversal as follows:

$$if\,\dot{m}_{wf,in,i} < 0 h_{wf,i} = h_{wf,in,i}$$

$$if\,\dot{m}_{wf,out,i} > 0 h_{wf,i} = h_{wf,out,i} \tag{4}$$

The heat transfer rate of the working fluid cell was determined as follows:

$$\dot{Q}_{wf,i} = \frac{1}{\frac{1}{\alpha_{wf,i}A_i} + \frac{R_w}{2}}\left(T_{w,i} - T_{wf,i}\right) \tag{5}$$

where α_{wf} is the heat transfer coefficient of the working fluid, R_w is the thermal resistance of the metal tube wall, A_i the tube inner heat transfer area and T_w is the temperature of the wall. The heat transfer coefficient of the working fluid depends on the phase of the working fluid: the Gnielinski-Dittus-Boelter correlation [58] was used for the single phase, whereas the Steiner correlation from the VDI Heat Atlas [59] was used for the two-phase region. A first order filter with time constant$t_{f,\alpha} = 1$ s was included in the calculation of the heat transfer to facilitate the numerical convergence of the solver when a cell changes phase:

$$\frac{d\alpha_{wf,i}}{dt} = \frac{-\alpha_{wf,i} + \alpha_{correlation}}{t_{f,\alpha}} \tag{6}$$

where $\alpha_{correlation}$ is the heat transfer coefficient calculated through the heat transfer correlation.

The dynamics of the metal tube wall are governed by the energy balance on the solid material as follows:

$$V_{w,i}\rho_{w,i}c_{w,i}\frac{dT_{w,i}}{dt} = -\dot{Q}_{wf,i} + \dot{Q}_{eg,i} \tag{7}$$

where V_w, ρ_w and c_w are the volume, density and specific heat of the wall, while $\dot{Q}_{eg}$ is the heat transfer rate between the exhaust gas cell and the wall cell. The heat exchanger tubes are made of stainless steel to avoid corrosion from the exhaust gas acidic compounds ($c_w = 450$ J/kgK and$\rho_w = 7900$ kg/m^3). Because of the low thermal inertia, dynamic effects in the exhaust gas cell are neglected, and the heat transfer rate of the exhaust gas cells is calculated as follows:

$$\dot{Q}_{eg,i} = \dot{m}_{eg}c_{p,eg,i}\left(1 - \exp\left\{-\frac{1}{\left[\frac{1}{\alpha_{eg,i}A_o\left(1+\frac{A_f}{A_o}\left(\eta_{f,i}-1\right)\right)} + \frac{R_w}{2}\right]\dot{m}_{eg}c_{p,eg,i}}\right\}\right)\left(T_{eg,in,i} - T_{w,i}\right) \tag{8}$$

where $\dot{m}_{eg,in}$ and $c_{p,g}$ are the mass flow rate and the gas specific heat at constant pressure. α_{eg} is the heat transfer coefficient of the exhaust gas, A_o is the heat transfer surface area of the bare tube, A_f is the heat transfer area of the fins and η_f is the fin efficiency. The heat transfer area of the bare tube A_o is defined as follows:

$$A_o = n_{tubes}l_i\pi d \tag{9}$$

where n_{tubes} is the number of tubes, l_i is the tube length and d is the outer tube diameter of the i-th gas cell. Given the fin outer diameter d_f, fin pitch f_{pitch} and fin thickness s, the heat transfer area of the fins (of radial type) is defined by

$$A_f = n_{tubes}\frac{l_i}{f_{pitch}}\left[2\frac{\pi\left(d_f{}^2 - d^2\right)}{4} + s\pi d_f\right] \tag{10}$$

The ratio $\frac{l_i}{f_{pitch}}$ corresponds to the number of fins per tube in the gas cell. For the exhaust gas, the correlation for heat transfer on the shell-side of tube bundles from the VDI Heat Atlas [60] was used. The fin efficiency was determined by using the method suggested by Schmidt [61].

Since the dynamics of the ORC unit are mainly governed by the heat exchangers, the turbine and the pump were modelled at steady-state [16]. Given the fact that ORC turbines typically work in sonic conditions, the turbine part-load characteristics was defined by the Stodola equation corrected for real gases [62]:

$$\dot{m}_{wf,2} = k_T\frac{p_{wf,2}}{\sqrt{\gamma_{wf,2}Z_{wf,2}T_{wf,3}}} \tag{11}$$

where $\dot{m}_{wf,2}$ is the mass flow rate of the working fluid, $p_{wf,2}$ is the pressure, $\gamma_{wf,2}$ is the ratio of the specific heats, $Z_{wf,2}$ is the compressibility factor and $T_{wf,2}$ is the temperature at turbine inlet. The constant $k_T = 0.128$ kg/s·K$^{0.5}$/kPa was determined from the design conditions. In the dynamic model, Eq. (11) was corrected by including a time filter with a small time constant $t_{f,T} = 0.1$ s in order to facilitate the convergence of the numerical problem:

$$\frac{d\dot{m}_{wf,2}}{dt} = \frac{-\dot{m}_{wf,2} + k_T\frac{p_{wf,2}}{\sqrt{\gamma_{wf,2}Z_{wf,2}T_{wf,3}}}}{t_{f,T}} \tag{12}$$

The time constant was chosen such that no significant impact on the ORC dynamics is detected. The isentropic efficiencies of the turbine and the pump (positive-displacement type) were corrected at part-load according to Refs. [63] and [64]. To simplify the control problem, the condenser was modelled by assuming constant temperature and

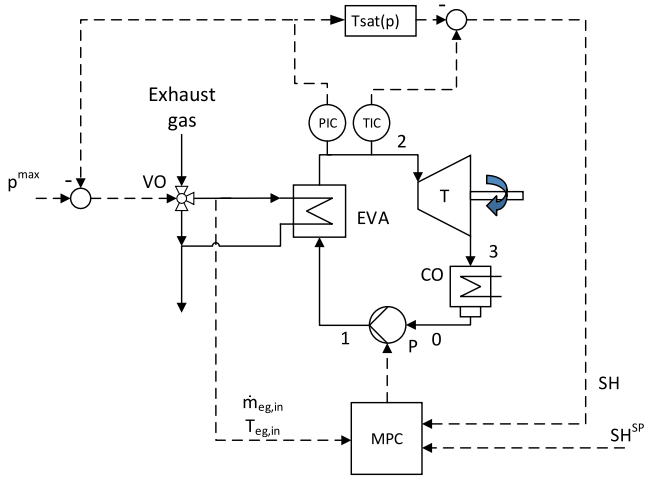

Fig. 2. Control logic diagram of the ORC unit.

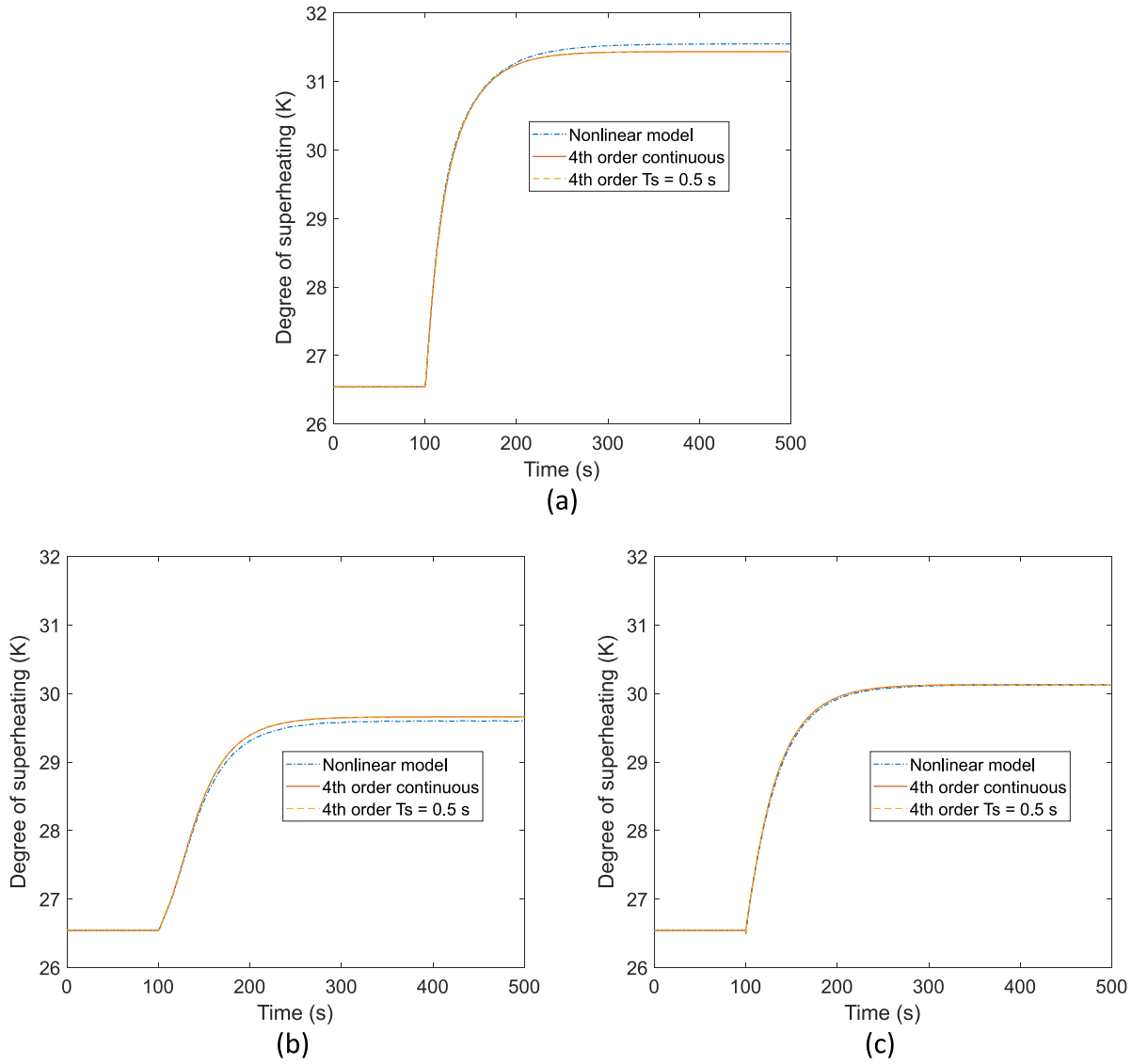

Fig. 3. Step response of the degree of superheating for the nonlinear full-order model and the reduced fourth-order models (continuous-time and discrete-time with sample time period of 0.5 s) to (a) a negative step change of 3 % in mass flow rate of the pump, (b) a positive step change of 3 % in mass flow rate of exhaust gas and (c) a positive step change of 5 K in inlet temperature of exhaust gas.

pressure of the working fluid, which is commonly done to simplify the complexity of the control problem [26,43]. Despite the model simplification, the MPC can handle variations in condensation conditions as an unmeasured disturbance and, hence, it can compensate for its influence on the controlled variable.

The state variables of the high pressure part of the ORC unit are the evaporator pressure $p_{wf,2}$ and the mass flow rate at turbine inlet $\dot{m}_{wf,2}$, as well as the specific enthalpies $h_{wf,i}$, the heat transfer coefficients $\alpha_{wf,i}$, and the wall temperatures $T_{w,i}$ of the 15 finite volume cells of the evaporator. In total there are 47 states describing the time evolution of the dynamic model.

3. Control model development and order reduction

The ORC control strategy is illustrated by Fig. 2. It is based on two separate controllers: i) a single-input–single-output (SISO) MPC that has the most complex task of keeping of the degree of superheating $SH_{wf,2}$ close to the desired set point SH^{SP} by rejecting the fluctuations of the mass flow rate $\dot{m}_{eg}$ and temperature $T_{eg,in}$ of the exhaust gas, and ii) a SISO proportional controller that limits the pressure $p_{wf,2}$ to the maximum value of 35 bar. The MPC acts on the mass flow rate of the pump $\dot{m}_{wf,1}$, while the proportional controller manipulates the opening of the exhaust bypass valve VO. The latter was tuned by using the Controller Design Toolbox from MATLAB® [65], leading to a proportional gain of -0.0036 kPa^{-1}. Here, no integral part is required by the controller, since its goal is only to avoid approaching the critical pressure of the working fluid rather than tracking a given pressure set point. Under normal operating conditions ($p_{wf,2} < 35$ bar), the controller is saturated at full opening ($VO = 100$ %).

The MPC design requires a dynamic model of the high-pressure part of the ORC system, which can be described by the following SISO nonlinear model with two measured disturbances:

$$\frac{dx}{dt} = f(x, \dot{m}_{wf,1}, d)$$

$$SH_{wf,2} = g(x, \dot{m}_{wf,1}, d) \tag{13}$$

where x is a vector of 47 states, f is the state function, and g is the output function. The measured disturbance vector d consists of the actual mass flow rate (i.e. the non-bypassed portion $VO \bullet \dot{m}_{eg}$) and the inlet tem-

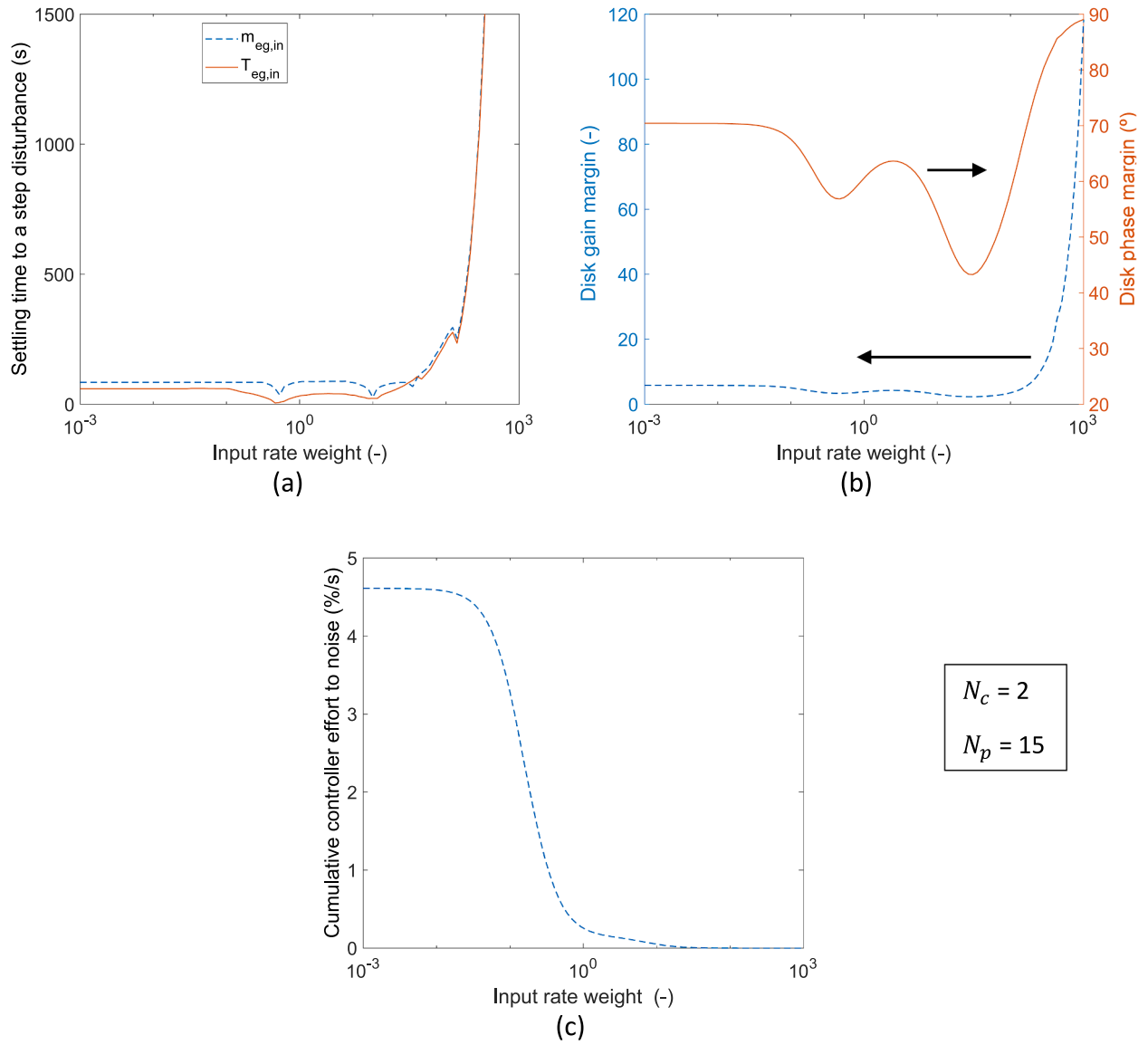

Fig. 4. Influence of the input rate weight on system performance and stability: a) settling time to 1 % step change in exhaust gas mass flow rate and 5 K step change in exhaust gas inlet temperature; b) disk margin and c) cumulative controller effort to noise of variance 0.01 K^2.

perature $T_{eg,in}$ of the exhaust gas. Subsequently, the nonlinear system in Eq. (2) is linearized around the steady-state nominal point $(x^*, \dot{m}^*_{wf,1}, d^*)$:

$$\frac{dx}{dt} = A(x - x^*) + B\left(\dot{m}_{wf,1} - \dot{m}^*_{wf,1}\right) + E(d - d^*)$$

$$SH_{wf,2} = C(x - x^*) + g(x^*, \dot{m}^*_{wf,1}, d^*) \tag{14}$$

where $A = \frac{\partial f}{\partial x}\Big|_{\left(x^*, \dot{m}^*_{wf,1}, d^*\right)}$, $B = \frac{\partial f}{\partial \dot{m}_{wf,1}}\Big|_{\left(x^*, \dot{m}^*_{wf,1}, d^*\right)}$, $C = \frac{\partial g}{\partial x}\Big|_{\left(x^*, \dot{m}^*_{wf,1}, d^*\right)}$ and $E = \frac{\partial f}{\partial d}\Big|_{\left(x^*, \dot{m}^*_{wf,1}, d^*\right)}$ are the partial derivatives of the state function and the output function calculated at nominal point. Since the degree of superheating at the evaporator outlet $SH_{wf,2}$ is defined by two states (the evaporator pressure $p_{wf,2}$ and the specific enthalpy of the last cell $h_{wf,N}$), $D = \frac{\partial g}{\partial \dot{m}^*_{wf,1}}\Big|_{\left(x^*, \dot{m}^*_{wf,1}, d^*\right)} = 0$ and $F = \frac{\partial g}{\partial d}\Big|_{\left(x^*, \dot{m}^*_{wf,1}, d^*\right)} = 0$.

The linear state-space model in Eq. (14) preserves the 47 states of the original nonlinear model in Eq. (13). This high number of states can lead to excessive computational time for a real-time implementation of the MPC. To prevent this, the order of the model is reduced. By subjecting the dynamic system to a 3 % step in mass flow rate of the pump $\dot{m}_{wf,1}$, it was found that four states are sufficient to limit the maximum deviation in degree of superheating $SH_{wf,2}$ to 0.2 K from the 47-state nonlinear model (see Fig. 3).

Smaller deviations (<0.1 K) are found subjecting the system to the measured disturbances d, i.e. a positive step change in mass flow rate (3 %) and a positive step in inlet temperature (5 K) of the exhaust gas. The reduction of the linearized system was carried out by using the 'balred' command of the Control System Toolbox from MATLAB® [65]. Next, the model is converted to a discrete-time model by using a zero-order hold with a sample time period $t_s = 0.5$ s (command 'c2d' from MATLAB® [65]):

$$x_{red,k+1} - x^* = e^{At_s}(x_{red,k} - x^*) + A^{-1}(e^{At_s} - I)\left(\dot{m}_{wf,1,k} - \dot{m}^*_{wf,1}\right) + A^{-1}(e^{At_s} - I)(d_k - d^*)$$

$$SH_{wf,2,k} = C(x_{red,k} - x^*) + g(x^*, \dot{m}^*_{wf,1}, d^*) \tag{15}$$

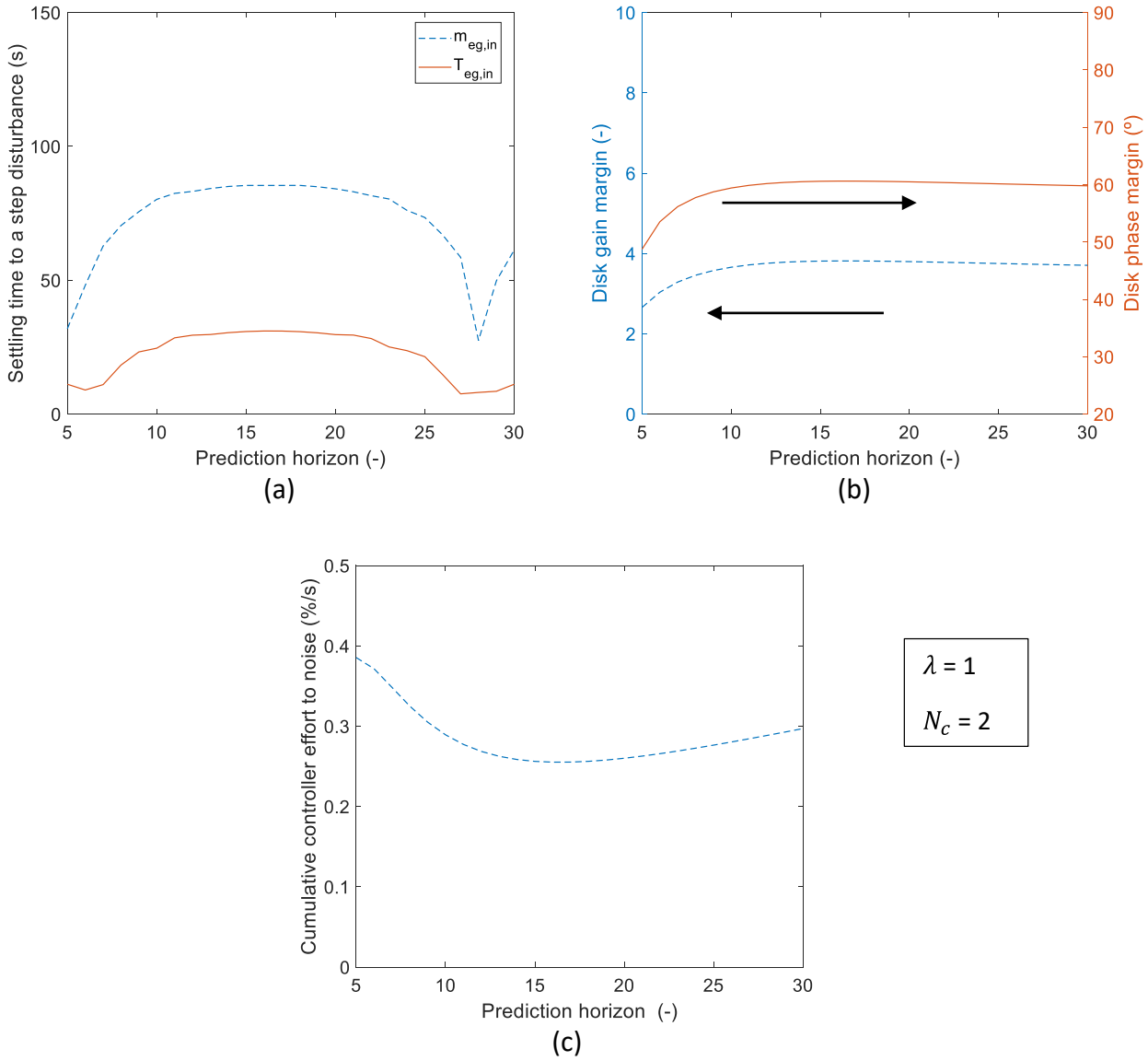

Fig. 5. Influence of the prediction horizon on system performance and stability: a) settling time to 1 % step change in exhaust mass flow rate and 5 K step change in exhaust temperature; b) disk margin and c) cumulative controller effort to noise of variance 0.01 K^2.

where k is the current time step, I is the identity matrix and the subscript 'red' refers to the reduced-order model.

4. Parameter tuning via multi-objective optimization

The fourth-order discrete-time linear system model described in Eq. (15) was used to tune the MPC system. The MPC formulation used in the work is available in the Model Predictive Control Toolbox from MATLAB® [65]. The controller objective function J and the constraint on the controller output are defined as follows:

$$J(\lambda,N_p,N_c)=\sum_{i=1}^{N_p}\left\{\frac{1}{SH^{ref}}\left[SH^{SP}-SH_{wf,2}(i)\right]\right\}^2+\lambda^2\sum_{i=1}^{N_c}\left\{\frac{1}{\dot{m}_{wf,1}^{ref}}\left[\Delta\dot{m}_{wf,1}(i)\right]\right\}^2$$

$$\dot{m}_{wf,1,min}\le\dot{m}_{wf,1}(i)\le\dot{m}_{wf,1,max}i=1,\cdots,N_c \tag{16}$$

where $SH^{ref}=20$ K is a scaling factor for the degree of superheating, $\dot{m}_{wf,1}^{ref}$=0.2 kg/s is a scaling factor for the pump mass flow rate and $\dot{m}_{wf,1,min}$ and $\dot{m}_{wf,1,max}$ correspond to 20 % and 120 % of the nominal mass flow rate of the ORC pump. The MPC tuning parameters are the input rate weight λ, the prediction horizon N_p and the control horizon N_c. A high value of the input rate weight λ penalizes changes in pump mass flow rate with respect to deviations of the degree of superheating from the desired set point, and vice versa. A high number of the prediction horizons include more time steps in the future when minimizing the deviation of the degree of superheating $SH_{wf,2}$ from the set point SH^{SP}, and vice versa. The control horizon defines the number of changes for the pump mass flow rate $\Delta\dot{m}_{wf,1}$ in the future. In the time steps $i>N_c$, the pump mass flow rate does not change anymore, i.e. $\Delta\dot{m}_{wf,1}(i>N_c)=0$. The sample time of the MPC corresponds to the sample time of the dynamic model ($t_s=0.5$ s).

4.1. Influence of the MPC tuning parameters

The influence of the tuning parameters λ, N_p and N_c on the control performance of the MPC system is evaluated considered the following quantities:

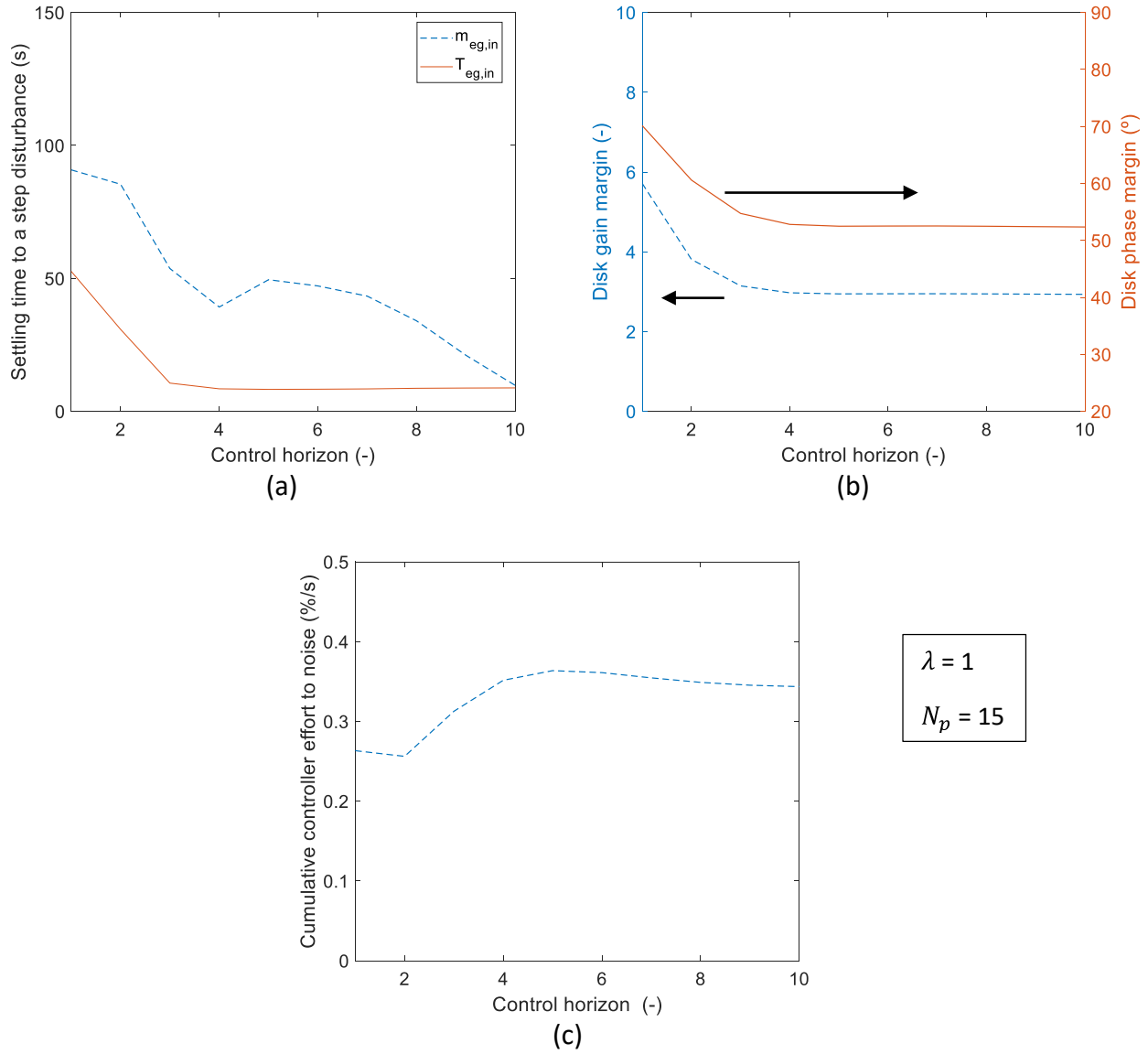

Fig. 6. Influence of the control horizon on system performance and stability: a) settling time to 1 % step change in exhaust mass flow rate and 5 K step change in exhaust temperature; b) disk margin and c) cumulative controller effort to noise of variance 0.01 K^2.

- The settling time $t_{SH,wf,2}$ of the degree of superheating due to a 1 % step change in mass flow rate of the exhaust gas $\dot{m}_{eg,in}$ and 5 K step change in inlet temperature of the exhaust gas $T_{eg,in}$. The settling time is the time required by the controller error (the deviation of the degree of superheating $SH_{wf,2}$) to fall below ± 2 % of the peak response value [66]. The shorter the settling time, the faster the controller can reject the disturbance;
- The disk margin, which gives information about the stability of the control system, also far from the operation point [67]. To ensure robustness against uncertainties and model deviations far from the nominal point, it is suggested to guarantee a disk gain margin above 2, and a disk phase margin above 45° [67];
- The cumulative controller effort due to noise in the measurement. For this purpose, white noise of variance 0.01 K^2 is added to $SH_{wf,2}$ before the measurement is fed back to the MPC, which quantifies the sensitivity of the MPC to measurement noise. The cumulative controller effort is determined as follows:

$$Q = \frac{1}{\left|\dot{m}_{wf,1,max} - \dot{m}_{wf,1,min}\right|} \frac{1}{\Delta t} \int_0^{\Delta t} \left| \frac{\Delta \dot{m}_{wf,1}}{t_s} \right| dt \tag{17}$$

where t is the time, Δt the overall time period of the simulation. The variance of the measurement noise is based on the experimental results reported in Ref. [52].

The sensitivity of the controller performance as a function of the tuning parameters was tested against the fourth-order discrete-time model. The analysis presented section 3 indicates that, for small deviations from the nominal point, the reduced-order discrete-time model represents with higher accuracy the behavior of the original nonlinear model in Eq. (15). The influence of the input rate weight λ on the settling time to a step disturbance, the disk margins and the cumulative controller effort to noise is shown in Fig. 4. Here, the control horizon and the prediction horizon were fixed to 2 and 15, respectively. Fig. 4a shows that the settling time $t_{SH,wf,2}$ to a step change in exhaust gas mass flow rate and inlet temperature has the same trend, and it can vary from 59 to 85 s at $\lambda = 10^{-3}$ up to 1500 s at $\lambda = 400$. This is because the input

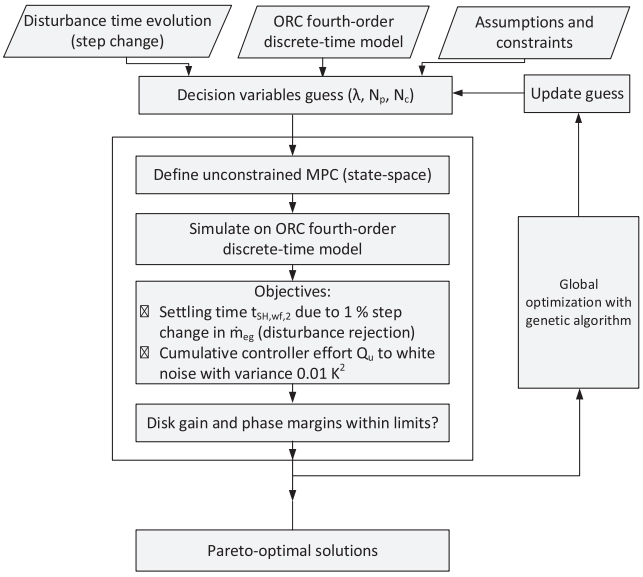

Fig. 7. Multi-objective optimization algorithm.

rate weight penalizes large variation of the manipulated variable $\dot{m}_{wf,1}$, and therefore the controller reaction to the disturbance step change is slower. At $\lambda < 10$ the settling time does not vary significantly, even though two minima occur. Concerning the closed-loop stability, higher input rate weights lead to increased disk gain (up to 120 at $\lambda = 1000$), while the disk phase margin fluctuates between 40° and 70° for $\lambda < 100$ before increasing up to 90° at $\lambda = 1000$. Input rate weights lower than 20 and higher than 40 satisfy both disk margin criteria for robustness (disk gain margin above 2 and disk phase margin above 45°). At last, Fig. 4c shows that a higher input rate weight is strongly beneficial to achieve a lower cumulative controller effort, which drops significantly in the region $10^{-1} < \lambda < 10$.

Fig. 5 shows the impact of the prediction horizon on the controller performance and the stability of the closed-loop system. Here, the input rate weight and the control horizon were fixed to 1 and 2, respectively. It can be seen that the settling time $t_{SH,wf,2}$ has a similar trend for a step change in exhaust gas mass flow rate and inlet temperature, although the variations for the step in exhaust gas mass flow rate are more pronounced. In this case, $t_{SH,wf,2}$ increases from 32 s to 85 s for a prediction horizon increase from 5 to 15, whereas $t_{SH,wf,2}$ drops down to 27.5 s from 16 s to 27 s, before increasing again for higher values of N_p. The closed-loop system is stable for the whole range of prediction horizons with both disk gain and phase margins increasing up to $N_p = 15$ and then staying constant. The cumulative controller effort decreases from 0.39 %/s to 0.26 %/s for N_p increasing from 5 to 15, and increases again to 0.3 %/s for N_p increasing from 16 to 30.

The influence of the control horizon on the closed-loop system response is shown in Fig. 6 for $\lambda = 1$ and $N_p = 15$. The settling time to a step change in exhaust gas mass flow rate is strongly reduced from 91 s to 9 s for N_c increasing from 1 to 10. The settling time to a step change in exhaust gas inlet temperature reduces considerably for N_c increasing from 1 to 4, before stabilizing at approximately 9 s. The reduced settling time for higher N_c is coupled with reduced disk gain and phase margins (although they both stayed above the recommended values of respectively 2 and 45°). Furthermore, the cumulative controller effort increases from 0.26 %/s to 0.36 %/s for N_c increasing from 2 to 5, and then it slightly drops until 0.34 %/s for $N_c = 10$.

The sensitivity analysis suggests that the settling time considerably increases for higher values of λ and low values of N_c, whereas the trend for N_p is not obvious. The disk gain and phase margin also increase for higher values of λ and N_p as well as low values of N_c. The cumulative controller effort decreases for higher values of λ whereas the trend is not

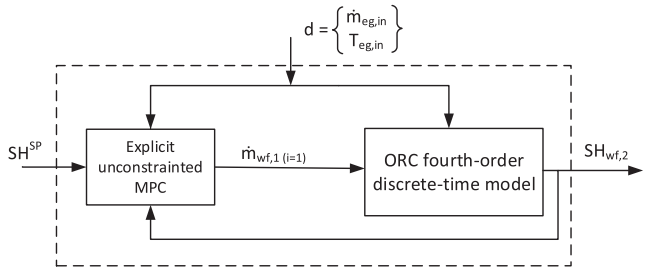

Fig. 8. Control scheme for the multi-objective optimization routine.

monotone for N_p and N_c. It should also considered that different combinations of the MPC tuning parameters λ, N_p and N_c would lead for the minimum/maximum objectives to shift for higher or lower values of the tuning parameters.

4.2. Multi-objective optimization routine

The previous section highlighted that the MPC tuning parameters λ, N_p and N_c can cause large variability of the settling time to a disturbance step change, of the stability margins and of the cumulative controller effort. In particular, the objectives of minimum settling time and minimum cumulative controller effort do not occur for the same set of MPC tuning parameters λ, N_p and N_c. In addition, the minimum objectives might be reached for sets that do not satisfy the conditions for robustness based on the disk margins. For this reason, a trade-off has to be found among the different objectives, excluding the solutions that do not ensure sufficient stability margins. To understand better the trade-off among the different objectives, a multi-objective optimization routine was developed (see Fig. 7). The routine receives as inputs the time evolution of the disturbance (a 1 % step change in exhaust gas mass flow rate), the fourth-order discrete-time model in Eq. (15) and the thresholds for sufficient robustness against model uncertainties (the disk gain margin has to be above 2 and the disk phase margin above 45°). A first guess of the MPC tuning parameters λ, N_p and N_c is also required, such that the multi-objective optimization can start. For the multi-objective optimization, the unconstrained MPC formulation with the objective function J in Eq. (16) was used. In other words, the constraint on the pump mass flow rate was not included in the MPC formulation. In this way, the MPC can be written explicitly as a linear time-invariant system having as inputs the measured degree of superheating $SH_{wf,2}$ and the measured disturbance vector d, while the output is the mass flow rate of the pump for the next time step $\dot{m}_{wf,1}(i = 1)$. The set point of the degree of superheating is kept constant at nominal value.

The control scheme is illustrated in Fig. 8. The explicit unconstrained MPC system that acts on the fourth-order discrete-time model described in section 3 is used to evaluate the objectives of the optimization. The two objectives of the multi-objective optimization routine are the following: i) the settling time of the degree of superheating $t_{SH,wf,2}$ due to a 1 % step change in the mass flow rate of the exhaust gas, which quantifies the disturbance rejection capabilities of the controller and needs to be minimized, and ii) the cumulative controller effort Q_{noise} when white noise of variance 0.01 K^2 is added to $SH_{wf,2}$ before the measurement is fed back to the MPC, which quantifies the sensitivity of the MPC to measurement noise and needs to be minimized as well. A high sensitivity to measurement noise, i.e. a high Q_{noise}, may lead to an excessive control action and reduced lifetime of the ORC pump and its automation system.

The genetic algorithm of the Global Optimization Toolbox from MATLAB® [47] is able to handle a combination of real (such as the input rate weight λ) and integer decision variables (such as the prediction horizon N_p and the control horizons N_c) and was, therefore, used as optimization algorithm. The settings for the algorithm are the following: i) a population size of 100, ii) 500 generations, and iii) a stall generation

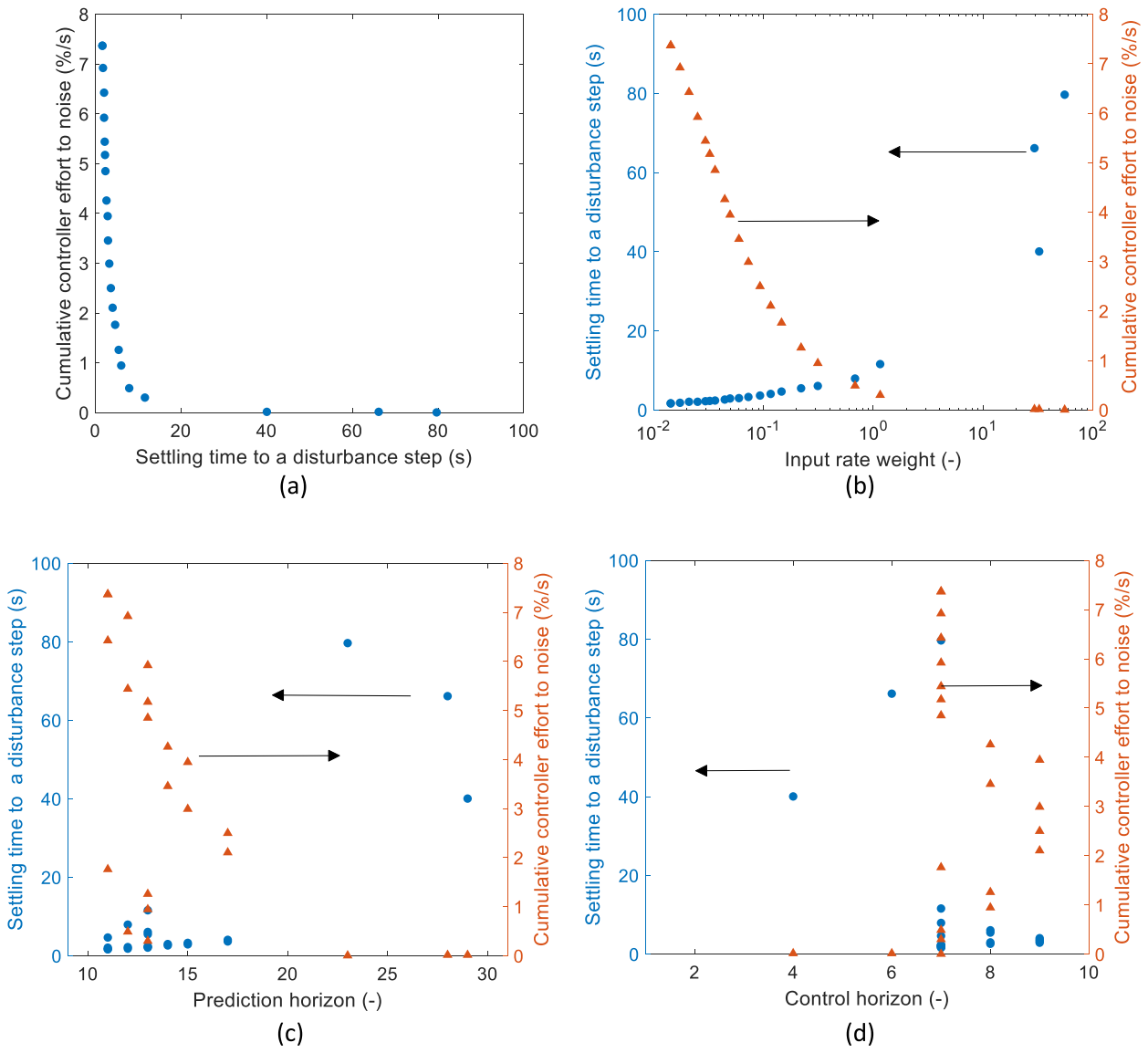

Fig. 9. (a) Pareto-front optimal solutions and influence of the optimal decision variables on the objective functions: (b) input rate weight, (c) prediction horizon and (d) control horizon.

limit of 200. The input rate weight λ can vary between 0.01 and 60, prediction horizon N_p can vary between 5 and 30, and the control horizon N_c can vary between 1 and 10. The results of the multi-objective optimization are discussed in the next section.

5. Optimization results

5.1. Multi-objective optimization

The results of the multi-objective optimization are located in a Pareto front of optimal solutions as depicted in Fig. 9a. It is important to highlight that Fig. 9a to 9d do not show the results of a sensitivity analysis (as previously carried out in section 4.1) but show the solutions of the multi-objective optimization problem, and therefore represent an optimal tuning of the controller parameters. The results in Fig. 9a suggest that a trade-off between the two objectives is required: low settling times $t_{SH,wf,2}$ imply high Q_{noise} and vice versa. The settling time $t_{SH,wf,2}$ is below 10 s for a cumulative controller effort above 0.3 %/s, although $t_{SH,wf,2}$ increases considerably to more than 100 s for a cumulative controller effort below 0.1 %/s. The decision variable that has the largest impact on the settling time $t_{SH,wf,2}$ and the cumulative controller effort Q_{noise} is the input rate weight λ, as shown by Fig. 9b, in agreement with the results of the sensitivity analysis in section 4.1. A higher λ implies a larger penalty on variations of the pump mass flow rate $\Delta\dot{m}_{wf,1}$, and therefore, the controller becomes more gentle, taking more time to reach the desired set point (larger $t_{SH,wf,2}$). At the same time, a more gentle reaction of the controller corresponds to a lower cumulative controller effort Q_{noise}. The prediction and the control horizons do not show a clear impact on the settling time and the cumulative controller effort, but the optimization still suggests an optimum range of selection (see Fig. 9c and 9d). The prediction horizon N_p varies in the range 10–17 for most of the points, but it is higher than 24 for points having a settling time $t_{SH,wf,2}$ of more than 30 s. No clear trend between N_p and Q_{noise} is found. The control horizon N_c is in the range of 7–9 for most of the optimal points having a settling time $t_{SH,wf,2}$ below 30 s, but it drops to 4 s for higher $t_{SH,wf,2}$. Analogously for the prediction horizon N_p, no clear trend is found between N_c and Q_{noise}.

5.2. Controller performance on finite volume nonlinear model

In a next step, the MPC design Pareto-front optimal solutions were

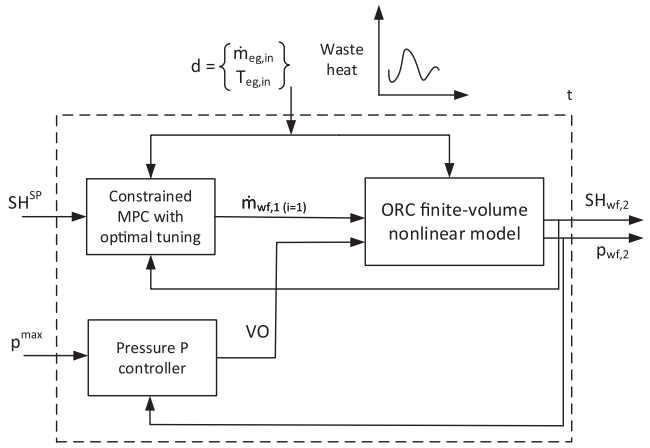

Fig. 10. Test setup for optimally tuned controllers.

tested on the nonlinear model of the high pressure part of the ORC unit described by Eq. (13), subjected with the realistic waste heat profile in Fig. 1b. The simulation setup is illustrated in Fig. 10. The mass flow rate of the pump $\dot{m}_{wf,1}$ was set by the MPC to keep the degree of superheating close to the design value while $\dot{m}_{wf,1}$ was constrained between 20 % and 120 % of the nominal value during the simulation. Additionally, as explained in the beginning of section 3, a proportional controller was used to manipulate the bypass valve opening to limit the pressure to the maximum value of 35 bar.

The response of the nonlinear system in Eq. (13) is assessed according to two quantities: i) the absolute root mean square tracking error (ARMSTE), quantifying the deviations between the degree of superheating $SH_{wf,2}$ and the set point SH^{SP}, and ii) the cumulative controller effort of the pump controller Q over the waste heat profile, see Eq. (17). The goal is to achieve the minimum ARMSTE as well as the minimum Q to reach good disturbance rejection while ensuring long lifetime of the pump. The results, plotted in Fig. 11a, indicate that there is a trade-off between the cumulative controller effort Q and the absolute root mean square tracking error ARMSTE over the profile analogously to the Pareto-front optimal solutions shown in Fig. 9a. The cumulative controller effort increases considerably from 1.1 %/s for an ARMSTE of

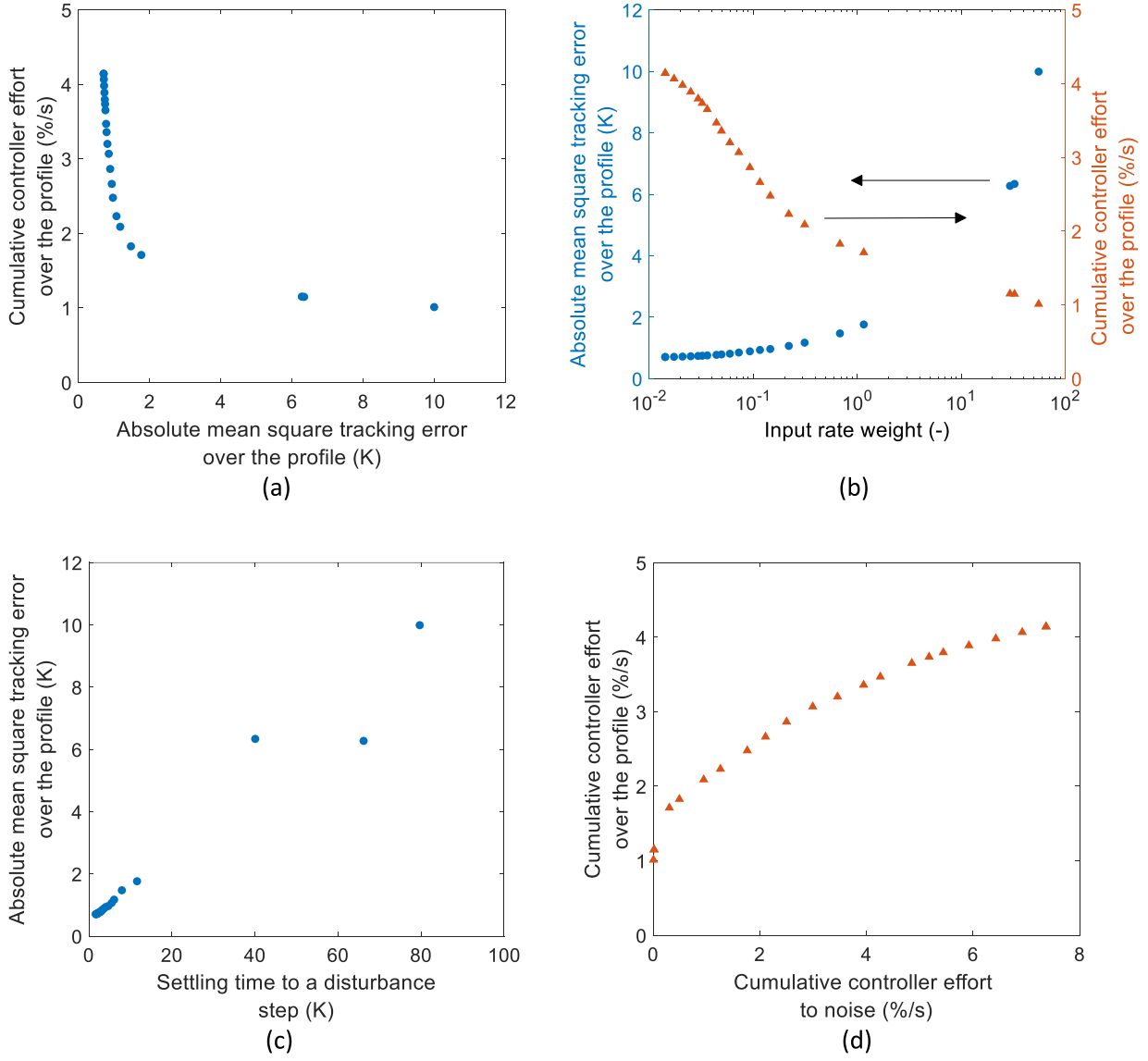

Fig. 11. (a) Cumulative controller effort and ARMSTE over the profile, (b) influence of the input rate weight, (c) ARMSTE as a function of the settling time to a disturbance step and (d) cumulative controller effort over the profile vs cumulative controller effort to noise.

about 6 K to more than 4 %/s for an ARMSTE below 2 K. Analogously to the results of the multi-objective optimization, the input rate weight λ has the largest impact on the simulation performance, as indicated in Fig. 11b. On the one hand, a low λ leads to a low ARMSTE because the controller can react very quickly to the waste heat fluctuations, although this leads to the highest cumulative controller effort Q. By increasing λ up to 55, Q drops to 1 %/s while the ARMSTE increases to 10 K. Importantly, it can be seen in Fig. 11c and 11d that there is a direct correlation between the settling time to a disturbance step $t_{S,SH,wf2}$ and the ARMSTE over the profile, as well as between the cumulative controller effort to noise Q_{noise} and over the profile Q. This means that important information about the controller performance over the realistic waste heat profile can be obtained from a less time-consuming analysis using a reduced-order model of the ORC system subjected to only a disturbance step change and measurement noise. This allow saving significant time and computational effort for the controller tuning. For an ARMSTE below 2 K, the settling time $t_{S,SH,wf2}$ should not exceed 15 s, while for Q below 2 %/s, *Qnoise* should be below 0.5 %/s.

6. Conclusions

This work focused on the control of an organic Rankine cycle unit recovering the waste heat available in the exhaust gas of a heavy-duty truck. Measurement data of the exhaust gas during a 45-min driving cycle of the truck were used as heat source of the organic Rankine cycle. The highly-transient heat source conditions require very powerful and effective controllers that can keep the operation of the organic Rankine cycle safe. This work focused on the design of a model predictive controller, based on a fourth-order discrete-time linear model of an organic. A multi-objective optimization approach was used to find the optimal tuning parameters of the model predictive controller. The performance of the optimal solutions was tested on a nonlinear model of the high pressure part of the organic Rankine cycle unit and on a realistic waste heat profile. The primary findings of the work can be summarized as follows:

- The optimization results suggest that there is a trade-off between the settling time of the degree of superheating at turbine inlet due to a step change in exhaust gas mass flow rate and the cumulative controller effort of the pump due to measurement noise. Both should be minimized for good controller performance and long component lifetime.
- The results indicate that the input rate weight is the tuning parameter with the largest influence on the controller performance, while the optimal prediction and control horizons should be in the range 10–17 and 7–9, respectively, for most of the optimal tuning sets.
- It was found that a direct relationship exists between the settling time of the degree of superheating at turbine inlet due to a disturbance step and the absolute root mean square tracking error over the profile. Also, the cumulative controller effort of the pump mass flow rate over the profile increases for higher cumulative controller effort of the pump mass flow rate due to measurement noise. Because of these dependencies, the trade-off between the settling time of the degree of superheating at turbine inlet due to a disturbance step change and the cumulative controller effort of the pump mass flow rate due to noise can be mapped into a trade-off between the absolute root mean square tracking error of the degree of superheating at turbine inlet and the cumulative controller effort of the pump mass flow rate over the profile.

Importantly, the multi-objective optimization routine presented in the paper can be used to identify the optimal model predictive controller parameters, considerably lowering the computational effort compared with that of an optimization based on the more complex nonlinear model. The presented method is a powerful tool to tune the design parameters of model predictive controllers in a more systematic and effective way compared with time-consuming, experience-based trial and error methods. Future work will evaluate the tuning of the controller parameters also in terms of net power output (considerations about the optimal degree of superheating at part-load are required) and the economic performance of the organic Rankine cycle unit will be evaluated.

Declaration of Competing Interest

The authors declare that they have no known competing financial interests or personal relationships that could have appeared to influence the work reported in this paper.

Data availability

The authors are unable or have chosen not to specify which data has been used.

Acknowledgements

This research was developed as part of the project “ACT-ORC: Advanced control of organic Rankine cycle for increased energy efficiency of heavy-duty trucks”, funded by the European Union’s Horizon 2020 research and innovation program under the Marie Sklodowska-Curie grant agreement no. 754462 (EuroTechPostdoc).

References

[1] S. Lion, C.N. Michos, I. Vlaskos, R. Taccani, A thermodynamic feasibility study of an Organic Rankine Cycle (ORC) for heavy-duty diesel engine waste heat recovery in off-highway applications, Int. J. Energy Environ. Eng. 8 (2017) 81–98, https://doi.org/10.1007/s40095-017-0234-8.
[2] H. Teng, G. Regner, C. Cowland, Achieving High Engine Efficiency for Heavy-Duty Diesel Engines by Waste Heat Recovery Using Supercritical Organic-Fluid Rankine, Cycle (2006), https://doi.org/10.4271/2006-01-3522.
[3] T. Park, H. Teng, G.L. Hunter, B. van der Velde, J. Klaver, A Rankine Cycle System for Recovering Waste Heat from HD Diesel Engines - Experimental Results, 2011. https://doi.org/10.4271/2011-01-1337.
[4] E.H. Wang, H.G. Zhang, B.Y. Fan, M.G. Ouyang, Y. Zhao, Q.H. Mu, Study of working fluid selection of organic Rankine cycle (ORC) for engine waste heat recovery, Energy 36 (2011) 3406–3418, https://doi.org/10.1016/j.energy.2011.03.041.
[5] V. Dolz, R. Novella, A. García, J. Sánchez, HD Diesel engine equipped with a bottoming Rankine cycle as a waste heat recovery system. Part 1: Study and analysis of the waste heat energy, Appl. Therm. Eng. 36 (2012) 269–278, https://doi.org/10.1016/j.applthermaleng.2011.10.025.
[6] D.T. Hountalas, G.C. Mavropoulos, C. Katsanos, W. Knecht, Improvement of bottoming cycle efficiency and heat rejection for HD truck applications by utilization of EGR and CAC heat, Energy Convers. Manag. 53 (2012) 19–32, https://doi.org/10.1016/j.enconman.2011.08.002.
[7] S. Quoilin, R. Aumann, A. Grill, A. Schuster, V. Lemort, H. Spliethoff, Dynamic modeling and optimal control strategy of waste heat recovery Organic Rankine Cycles, Appl. Energy 88 (2011) 2183–2190, https://doi.org/10.1016/j.apenergy.2011.01.015.
[8] P. Tona, J. Peralez, Control of Organic Rankine Cycle systems on board heavy-duty vehicles: A survey, IFAC-PapersOnLine 28 (2015) 419–426, https://doi.org/10.1016/j.ifacol.2015.10.060.
[9] J. Zhang, K. Li, J. Xu, Recent developments of control strategies for organic Rankine cycle (ORC) systems, Trans. Inst. Meas. Control 41 (2019) 1528–1539, https://doi.org/10.1177/0142331217753061.
[10] M. Jiménez-Arreola, R. Pili, C. Wieland, A. Romagnoli, Analysis and comparison of dynamic behavior of heat exchangers for direct evaporation in ORC waste heat recovery applications from fluctuating sources, Appl. Energy 216 (2018) 724–740, https://doi.org/10.1016/j.apenergy.2018.01.085.
[11] G. Carraro, R. Pili, A. Lazzaretto, F. Haglind, Effect of the evaporator design parameters on the dynamic response of organic Rankine cycle units for waste heat recovery on heavy-duty vehicles, Appl. Therm. Eng. 198 (2021), 117496, https://doi.org/10.1016/j.applthermaleng.2021.117496.
[12] D. Tillmanns, J. Petzschmann, J. Schilling, C. Gertig, A. Bardow, ORC on tour: Integrated design of dynamic ORC processes and working fluids for waste-heat recovery from heavy-duty vehicles, 2019, p. 163–8. https://doi.org/10.1016/B978-0-12-818634-3.50028-X.
[13] R. Pili, S. Bojer Jørgensen, F. Haglind, Multi-objective optimization of organic Rankine cycle systems considering their dynamic performance, Energy 246 (2022), 123345, https://doi.org/10.1016/j.energy.2022.123345.

[14] B. Xu, D. Rathod, A. Yebi, Z. Filipi, S. Onori, M. Hoffman, A comprehensive review of organic rankine cycle waste heat recovery systems in heavy-duty diesel engine applications, Renew. Sustain. Energy Rev. 107 (2019) 145–170, https://doi.org/10.1016/j.rser.2019.03.012.

[15] S. Lion, C.N. Michos, I. Vlaskos, C. Rouaud, R. Taccani, A review of waste heat recovery and Organic Rankine Cycles (ORC) in on-off highway vehicle Heavy Duty Diesel Engine applications, Renew. Sustain. Energy Rev. 79 (2017) 691–708, https://doi.org/10.1016/j.rser.2017.05.082.

[16] M. Imran, R. Pili, M. Usman, F. Haglind, Dynamic modeling and control strategies of organic Rankine cycle systems: Methods and challenges, Appl. Energy 276 (2020), https://doi.org/10.1016/j.apenergy.2020.115537.

[17] D. Jolevski, O. Bego, P. Sarajcev, Control structure design and dynamics modelling of the organic Rankine cycle system, Energy 121 (2017) 193–204, https://doi.org/10.1016/j.energy.2017.01.007.

[18] M. Marchionni, G. Bianchi, A. Karvountzis-Kontakiotis, A. Pesyridis, S.A. Tassou, An appraisal of proportional integral control strategies for small scale waste heat to power conversion units based on Organic Rankine Cycles, Energy 163 (2018) 1062–1076, https://doi.org/10.1016/j.energy.2018.08.156.

[19] S. Lin, L. Zhao, S. Deng, J. Ni, Y. Zhang, M. Ma, Dynamic performance investigation for two types of ORC system driven by waste heat of automotive internal combustion engine, Energy 169 (2019) 958–971, https://doi.org/10.1016/j.energy.2018.12.092.

[20] C. Yang, W. Wang, H. Xie, An efficiency model and optimal control of the vehicular diesel exhaust heat recovery system using an organic Rankine cycle, Energy 171 (2019) 547–555, https://doi.org/10.1016/j.energy.2018.12.219.

[21] F. Padula, R. Sandrini, G. Cominardi, Adaptive PI control of an organic Rankine cycle power plant. vol. 2. IFAC; 2012. https://doi.org/10.3182/20120328-3-it-3014.00078.

[22] J. Peralez, P. Tona, O. Lepreux, A. Sciarretta, L. Voise, P. Dufour, et al., Improving the control performance of an organic rankine cycle system for waste heat recovery from a heavy-duty diesel engine using a model-based approach, Proc IEEE Conf Decis Control (2013) 6830–6836, https://doi.org/10.1109/CDC.2013.6760971.

[23] M. Usman, M. Imran, D.H. Lee, B.S. Park, Experimental investigation of off-grid organic Rankine cycle control system adapting sliding pressure strategy under proportional integral with feed-forward and compensator, Appl. Therm. Eng. 110 (2017) 1153–1163, https://doi.org/10.1016/j.applthermaleng.2016.09.021.

[24] M. Keller, M. Neumann, K. Eichler, S. Pischinger, D. Abel, T. Albin, Model predictive control for an organic rankine cycle system applied to a heavy-duty diesel engine, CCTA 2020–4th IEEE Conf. Control Technol. Appl. 442–9 (2020), https://doi.org/10.1109/CCTA41146.2020.9206319.

[25] Y. Vaupel, J.C. Schulze, A. Mhamdi, A. Mitsos, Nonlinear model predictive control of organic Rankine cycles for automotive waste heat recovery: Is it worth the effort? J. Process Control 99 (2021) 19–27, https://doi.org/10.1016/j.jprocont.2021.01.003.

[26] D. Seitz, O. Gehring, C. Bunz, M. Brunschier, O. Sawodny, Model-based control of exhaust heat recovery in a heavy-duty vehicle, Control Eng. Pract. 70 (2018) 15–28, https://doi.org/10.1016/j.conengprac.2017.08.010.

[27] R. Pili, C. Wieland, H. Spliethoff, F. Haglind, Numerical analysis of feedforward concepts for advanced control of organic Rankine cycle systems on heavy-duty vehicles, J. Clean. Prod. 351 (2022), 131470, https://doi.org/10.1016/j.jclepro.2022.131470.

[28] D. Luong, T.C. Tsao, Linear Quadratic Integral control of an Organic Rankine Cycle for waste heat recovery in heavy-duty diesel powertrain, Proc. Am. Control Conf. (2014) 3147–3152, https://doi.org/10.1109/ACC.2014.6858907.

[29] J. Zhang, M. Ren, H. Yue, Constrained entropy-based temperature control of waste heat systems, Proc. World Congr. Intell. Control Autom. 2016, 2016-Septe:1992–8. https://doi.org/10.1109/WCICA.2016.7578809.

[30] J. Zhang, X. Tian, Z. Zhu, M. Ren, Data-driven superheating control of organic Rankine cycle processes, Complexity 2018 (2018), https://doi.org/10.1155/2018/4154019.

[31] J. Peralez, P. Tona, A. Sciarretta, P. Dufour, M. Nadri, Optimal control of a vehicular organic rankine cycle via dynamic programming with adaptive discretization grid, vol. 19. IFAC; 2014. https://doi.org/10.3182/20140824-6-za-1003.02185.

[32] E. Feru, F. Willems, B. de Jager, M. Steinbuch, Modeling and control of a parallel waste heat recovery system for Euro-VI heavy-duty diesel engines, Energies 7 (2014) 6571–6592, https://doi.org/10.3390/en7106571.

[33] V. Grelet, P. Dufour, M. Nadri, V. Lemort, T. Reiche, Explicit multi-model predictive control of a waste heat Rankine based system for heavy duty trucks, Proc. IEEE Conf. Decis. Control 2015, 54rd IEEE:179–84. https://doi.org/10.1109/CDC.2015.7402105.

[34] A. Hernandez, A. Desideri, C. Ionescu, S. Quoilin, V. Lemort, R. De Keyser, Increasing the efficiency of Organic Rankine Cycle technology by means of multivariable, Predictive Control, vol. 19. IFAC; 2014. https://doi.org/10.3182/20140824-6-za-1003.01796.

[35] E.F. Camacho, C. Bordons, Model Predictive control. London: Springer London; 2007. https://doi.org/10.1007/978-0-85729-398-5.

[36] A. Hernandez, A. Desideri, C. Ionescu, S. Quoilin, V. Lemort, R. De Keyser, Experimental study of Predictive Control strategies for optimal operation of Organic Rankine Cycle systems, 2015 Eur. Control Conf. ECC 2015, 2015, 2254–2259. https://doi.org/10.1109/ECC.2015.7330874.

[37] A. Hernandez, A. Desideri, C. Ionescu, R. De Keyser, V. Lemort, S. Quoilin, Real-time optimization of organic Rankine cycle systems by extremum-seeking control, Energies (2016) 9, https://doi.org/10.3390/en9050334.

[38] A. Hernandez, F. Ruiz, S. Gusev, R. De Keyser, S. Quoilin, V. Lemort, Experimental validation of a multiple model predictive control for waste heat recovery organic Rankine cycle systems, Appl. Therm. Eng. 193 (2021), 116993, https://doi.org/10.1016/j.applthermaleng.2021.116993.

[39] J. Zhang, T. Zhang, M. Lin, G. Hou, K. Li, Multiple model predictive control for organic rankine cycle (ORC) based waste heat energy conversion systems, 2016 UKACC Int. Conf. Control UKACC Control 2016, 2016, 1–7. https://doi.org/10.1109/CONTROL.2016.7737577.

[40] L. Pierobon, R. Chan, X. Li, K. Iyengar, F. Haglind, E. Ydstie, Model Predictive Control of Offshore Power Stations with Waste Heat Recovery, J. Eng. Gas Turbines Power (2016) 138, https://doi.org/10.1115/1.4032314.

[41] D. Luong, T. Tsao, Model Predictive Control of Organic Rankine Cycle for Waste Heat Recovery in Heavy-Duty Diesel Powertrain, Proc. ASME 2014 Dyn. Syst. Control Conf. DSCC2014 2014:1–7.

[42] X. Liu, A. Yebi, P. Anschel, J. Shutty, B. Xu, M. Hoffman, et al., Model Predictive Control of an Organic Rankine Cycle System, Energy Procedia 129 (2017) 184–191, https://doi.org/10.1016/j.egypro.2017.09.109.

[43] H. Koppauer, W. Kemmetmüller, A. Kugi, Model predictive control of an automotive waste heat recovery system, Control Eng. Pract. 81 (2018) 28–42, https://doi.org/10.1016/j.conengprac.2018.09.005.

[44] D. Rathod, B. Xu, Z. Filipi, M. Hoffman, An experimentally validated, energy focused, optimal control strategy for an Organic Rankine Cycle waste heat recovery system, Appl. Energy 256 (2019), 113991, https://doi.org/10.1016/j.apenergy.2019.113991.

[45] B. Houska, H.J. Ferreau, M. Diehl, ACADO toolkit-An open-source framework for automatic control and dynamic optimization, Optim. Control Appl. Methods 32 (2011) 298–312, https://doi.org/10.1002/oca.939.

[47] Mathworks®. MATLAB® 2019.

[48] S. Trabucchi, C. De Servi, F. Casella, P. Colonna, Design, Modelling, and Control of a Waste Heat Recovery Unit for Heavy-Duty Truck Engines, Energy Procedia 129 (2017) 802–809, https://doi.org/10.1016/j.egypro.2017.09.140.

[49] A.P. Weiß, Volumetric Expander versus Turbine – Which is the Better Choice for Small ORC Plants? 3rd Int. Semin. ORC Power Syst. Oct. 12-14, 2015, Brussels, Belgium, 2015.

[50] L. Guillaume, A. Legros, A. Desideri, V. Lemort, Performance of a radial-inflow turbine integrated in an ORC system and designed for a WHR on truck application: An experimental comparison between R245fa and R1233zd, Appl. Energy 186 (2017) 408–422, https://doi.org/10.1016/j.apenergy.2016.03.012.

[51] F. Alshammari, A. Pesyridis, A. Karvountzis-Kontakiotis, B. Franchetti, Y. Pesmazoglou, Experimental study of a small scale organic Rankine cycle waste heat recovery system for a heavy duty diesel engine with focus on the radial inflow turbine expander performance, Appl. Energy 215 (2018) 543–555, https://doi.org/10.1016/j.apenergy.2018.01.049.

[52] R. Pili, S. Eyerer, F. Dawo, C. Wieland, H. Spliethoff, Development of a non-linear state estimator for advanced control of an ORC test rig for geothermal application, Renew. Energy (2020), https://doi.org/10.1016/j.renene.2020.07.121.

[53] F. Dawo, S. Eyerer, R. Pili, C. Wieland, H. Spliethoff, Experimental investigation, model validation and application of twin-screw expanders with different built-in volume ratios, Appl. Energy 282 (2021), 116139, https://doi.org/10.1016/j.apenergy.2020.116139.

[54] E. Macchi, M. Astolfi, Organic Rankine Cycle (ORC) Power Systems, Elsevier (2017), https://doi.org/10.1016/C2014-0-04239-6.

[55] Dassault Systèmes. Dymola 2020.

[56] TLK Thermo GmbH. TIL Suite 2016.

[57] Dassault Systèmes. FMI Kit for Simulink 2.0 2018.

[58] R. Pili, A. Romagnoli, M. Jiménez-Arreola, H. Spliethoff, C. Wieland, Simulation of Organic Rankine Cycle – Quasi-steady state vs dynamic approach for optimal economic performance, Energy (2019), https://doi.org/10.1016/j.energy.2018.10.166.

[59] M. Kind, D. Steiner, J.M. Chawla, J.-J. Schröder, Y. Saito, H. Auracher, et al., H3 Flow Boiling. VDI Heat Atlas, Berlin, Heidelberg: Springer Berlin Heidelberg; 2010, p. 793–902. https://doi.org/10.1007/978-3-540-77877-6_124.

[60] E.S. Gaddis, V. Gnielinski, G8 Shell-Side Heat Transfer in Baffled Shell-and-Tube Heat Exchangers. VDI Heat Atlas, Berlin, Heidelberg: Springer Berlin Heidelberg; 2010, p. 731–42. https://doi.org/10.1007/978-3-540-77877-6_41.

[61] T.E. Schmidt, La Production Calorifique des Surfaces Munies D'ailettes. Annex Du Bull L'institut Int Du Froid 1945;Annex G-5.

[62] F. Capra, E. Martelli, Numerical optimization of combined heat and power Organic Rankine Cycles - Part B: Simultaneous design & part-load optimization, Energy 90 (2015) 329–343, https://doi.org/10.1016/j.energy.2015.06.113.

[63] C. Vetter, Thermodynamische Auslegung und transiente Simulation eines überkritischen Organic Rankine Cycles für einen leistungsoptimierten Betrieb, KIT Karsluhe, 2014.

[64] G. Bauer, Ölhydraulik (Paragraph 5.3, Figure 5.26), Springer Fachmedien Wiesbaden, Wiesbaden, 2016, 10.1007/978-3-658-12344-4.

[65] Mathworks®. Control System Toolbox™, MATLAB® 2019.

[66] J.-P. Corriou, Process Control. London: Springer London; 2004. https://doi.org/10.1007/978-1-4471-3848-8.

[67] P. Seiler, A. Packard, P. Gahinet, An Introduction to Disk Margins [Lecture Notes], IEEE Control Syst. 40 (2020) 78–95, https://doi.org/10.1109/MCS.2020.3005277.